Single image defocus estimation by modified gaussian function

Author One*[1] | Author Two[2,3] | Author Three[3]

[1]Org Division, Org name, State name,
 Country name
[2]Org Division, Org name, State name,
 Country name
[3]Org Division, Org name, State name,
 Country name

Correspondence
*Corresponding author name, Corresponding
address. Email: authorone@Email.com

Present Address
Present address

Abstract

This article presents an algorithm to estimate the defocus blur from a single image. Most of the existing methods estimate the defocus blur at edge locations which further involves the reblurring process. For this purpose existing methods use the traditional Gaussian function in the phase of reblurring but it is found that the traditional Gaussian kernel is sensitive to the edges and can cause loss of edges information. Hence there are more chances of missing spatially varying blur at edge locations. We offered the repeated averaging filters as an alternative to the traditional Gaussian function which is more effective and estimate the spatially varying defocus blur at edge locations. By using repeated averaging filters, a blur sparse map is computed. The obtained sparse map is propagated by integration of superpixels segmentation and transductive inference to estimate full defocus blur map. Our adopted method of repeated averaging filters affects both the computational time of defocus blur map estimation and visual results of the final defocus recovered map.

KEYWORDS:
Defocus Blur; Defocus Map; Gaussian Smoothing; Integral Image

1 | INTRODUCTION

Defocus blur estimation is an important task in computer vision and computer graphics applications [1,2] and provides important clues for relative depth estimation. The defocus blur estimation and depth information recovery from two-dimensional images plays an important role which can offer aid for applications such as recognizing and detecting an object, understanding of a scene, obstacle avoidance inspection, refocusing, segmenting, matting, object tracking, depolarization of background, salient region detection and assembly [3–7]. Similarly its usefulness is also ideal for IOT based applications, such as use in wearable devices, video doorbells, and in surveillance products. Estimating the defocus blur and relative depth one needs to estimate blur in a defocus image.

Blur is a sort of noise and mostly images polluted by the blur or noise which can be referred to disturbances in data. These disturbances are of no interest and can limit the processing of images. Blur in image can be caused by camera shake [8,9]; motion of the object and phenomena of defocus [2,4,9–13]. Many pictures are captured with a sharp foreground and defocus background [1]. The reason for this is the focus and out of focus planes of the camera sensor. The object which lies on the focus plane results in a sharper image but if the object distance deviates from the focal plane causes a blurred image. This sort of blur can be referred to defocus blur. The human eye has the best structure which automatically percepts the focus and defocus objects in scene or image but for a sensor, it is difficult to percept the clarity of the objects in scenes.

Defocus blur estimation process contains two phases one to estimate the sparse map and the second one is the sparse map propagation into the whole image. In this article, we are focusing on a challenging problem of defocus blur map estimation from a single image. The defocus blur estimation methods fall into two main categories: multiple images based methods [14–17] and

single image based methods [18,19]. Multiple image based methods use more than one image captured by multiple camera focus settings, while the single image based methods use edges locations to estimate the defocus blur. Multiple images based methods suffered from some serious problems like occlusions and the scene should be static which practically limits their applications. On the other hand, recovering defocus from a single image is more practical.

Single image defocus blur estimation techniques mainly categorized into two classes i.e. gradient based methods [4,10–13,20,21] and frequency based methods [1,18,22–25]. The stated classes is further narrowed into two sub-classes; the first one is edge based [19,26–29] methods and the second one is region based method [30]. In edge based methods blur estimation is performed at edge locations. Edges based methods have proven to be fast as compared to region based methods. In region based methods, the defocus blur is recovered directly from the local patches of the input image. Region based methods showed much accurate blur maps [31] as compare to edge based methods.

Our method is edge based and inspired by Zhuo et al [19] proposed technique, which applied normal Gaussian blur kernel for re-blurring the input blur image. Then the ratio of gradients of input blur image and the reblurred image is computed. The offered approach was computationally expensive and resulted in loss of some edges after applying the normal Gaussian distribution. We planned a fast defocus map estimation system to encounter aforementioned drawbacks. Our proposed scheme adopts a modified Gaussian function on the basis of repeated averaging filters which result in a better sparse map at low computational cost and keeps much of edge information alive.

The repeated averaging filters which is the approximation of traditional Gaussian function can be used as a modified blur function instead of traditional Gaussian distribution. Our scheme uses the integral image theory, a proved concept for fast processing. In the subsequent step, computed the gradient ratio of the input blurred image and integral reblurred image. Attaining the gradient magnitude ratio we acquired the sparse map easily with ample edges preserving characteristics. To propagate the sparse map for getting the full defocus map we adopted the method of Chen et al [27] which further contains two phases of over-segmentation and transductive inference. Integrating the repeated averaging filters with Zhuo et al [19] and Chen et al [27] into one pipeline achieved a full defocus blur map recovery. The proposed method surpasses many states of the art techniques previously.

2 | RELATED WORK

Broad work has been done previously related to defocus estimation. Jiang et al [4] proposed a gradient related scheme, based on saliency detection, which aims to detect better regions for complex structures and integrated three visual clues such as focusness, uniqueness, and objectness. Focusness refers to, in pictures some region photographed are focused, and while uniqueness refers to-Visual contrast of the appearance of the objects and the third one was objectness which is-Complete boundaries of objects. Elder and Zucker [10] detected, localized and characterized the edges in the presence of blur by use of first and second order derivatives of the input image, which naturally leads to estimate the edge blur locally. Bae and Durand [11] defocus magnifying approach was based on blur kernel estimation at edge locations and gave a new direction to the sparse defocus map by making it full defocus map through interpolation method.

Namboodiri and Chaudhuri [12] estimated the blur by formulating the reverse heat equation. On the other hand, the reverse heat equation had the parabolic nature which is divergent. To balance the reverse heat equation they considered gradient degeneration and obtained the depth estimate. However, this method was not applicable to those regions which have less texture so further he refined the obtained depth map by Markov random field by using the MAP-MRF framework. Peng et al [13] estimated the scene depth for underwater images which observed that more blurriness is a result of the larger scene and therefore measured the scene depth. Integrating the image formation model (IFM) with blur, the depth estimate is attained by computing the distance between scene points and the camera. Tai and Brown [20] used the local contrast prior to estimate defocus map by considering image gradients locally. Their observations were based on the fact that images with defocus blur regions have smaller gradient magnitudes than the local contrast as a result of the blurring process. For propagating the defocus blur their proposed method described the Markov Random Field formulation.

Tang et al [1] advocated a procedure related to frequency based methods which targeted the spectrum amplitude of edges. For assessing defocus blur amount a full defocus map is projected. Liu et al [18] offered an analysis framework for partial blur detection and detected images having blurred regions. Their proposed system also added some extra features such as recognizing different types of blur without the use of the blur kernel. The suggested procedure was based on modeling the image color, spectral information, and gradient. Wang et al [22] proposed a region based algorithm. They used segmentation for classifying each block of the observed blurred image into background and foreground via average intensity and variance wavelets coefficients.

The average intensity was deliberated for similarity with corresponding image blocks. The variance of wavelets coefficients performed the background and foreground differentiation which is considered the main feature of the deliberated method. Kim et al [23] transformed the low depth of field (DOF) image into higher order statistics (HOS) space first. Secondly, they computed the HOS map and aloof the dark dumps by a morphological filter. Lastly, the object of interest was achieved through region merging and thresholding. Kovacs et al [24] suggested a classification methodology built on blind deconvolution to approximate the focused regions in common images. Saxena and Chung [25] computed a depth map on the basis of discriminatively-trained Markov Random Field (MRF) which was a supervised learning approach.

Recently many researches concentrated on the edge based methods which further consider reblurring the gradient magnitude ratios. Zhuo et al [19] anticipated technique first reblurred the input image by using Gaussian kernel. After that the gradient magnitude ratio of input image and reblurred image is computed to obtain raw sparse map. The raw sparse map is refined further by a joint bilateral filtering method. For sparse map propagation, they applied the matting Laplacian formulation. In the method of Pi and Zhang [26] a very simple approach is adopted and defocus blur is directly computed from the local gradients. The blur is computed at edge location using the gradient ratio on different scales. Furthermore the defocus blur is re-computed and for this purpose variance of the Gaussian gradient profiles is used. Chen et al [27] followed the same method of [19] for estimating the blur spare map and introduced the over-segmentation and transductive inference to propagate the sparse map robustly. Cao and Fang [28] designed scheme first a point to point defocus model is presented. Further a sparse map is estimated and propagated in two steps. For sparse map estimation a sharp edge prior is used and computed the blur at edge locations. A guided image is applied for propagation of the sparse map. Recently Zhang et al [29] proposed a method, they estimated the blur map by using edge information and K nearest neighbors (KNN) matting interpolation. Then the blur map is segmented for derivation of local kernels. Finally, they restored the latent image by adopting the BM3D-based non-blind deconvolution process.

Most of the above edge based techniques used the traditional Gaussian function which previously considered better accounts for its various anomalies in practical imaging systems, and had been used widely in depth from defocus, but applying the traditional Gaussians cause some loss of image information such as vanishing of weak edges in sparse to defocus as well as final defocus map. This intuition leads us to replace the traditional Gaussian by repeated averaging filters to recover defocus map by estimating the blur amount from a blurred image.

The rest of this paper is organized as follows. Defocus model is introduced in subsection 2.1.We discussed our approach in Section 3. The evaluations and results are discussed in Section 4. Section 5 concludes the overall approach used for defocus blur estimation.

2.1 | Defocus Model

In many cases, we need smaller defocus that can be regarded as useful for image manipulations. Focus and defocus is associated with the camera lens diameter which suggests that having smaller lenses produce less defocus and causing less blurry backgrounds. Contrary larger aperture lenses produce larger defocus. Detecting an edge is part of segmentation and goal is to produce a line like drawing from an image of a scene. We consider step edges for estimating the defocus blur at edge locations. For step images, the intensity changes abruptly which is shown in the Figure 1. Defocus blur can be estimated at edge locations. Natural images considers step edges as main edges, mathematically representation is given as

$$E(z) = AlphaU(z) + Beta \tag{1}$$

Where $U(z)$ stands for the step function, *Alpha* is the amplitude and *Beta* is the offset of the edge. Note that, edge is positioned at *z=0*. Focus and defocus comply with thin lens model that is assumed by [32]. Placing an object at focus distance *DF* (distance of focus), all emissions from the point of an object will congregate to a single sensor point and results in sharp image. When the object is lying on out of focus distance *D* (out of focus), rays will project on multiple sensor points and fallouts in a blurred image which depends on the shape of aperture and called circle of confusion *(COC)*. The diameter of *(COC)* describes the amount of defocus and written as

$$C = \frac{|D - DF|}{D} \frac{Fo}{n(D - DF)} \tag{2}$$

Where *Fo* signifies focal length and *n* referred as the stop number of the camera. Thin lens model depicted in Figure 2 shows focus and defocus for thin lens model and variation of diameter of circle of confusion which changes with respect to *D* and *n*, for a certain fixed *Fo* and *DF* [32]. The defocus image is convolution of sharp image and point spread function which is defined as

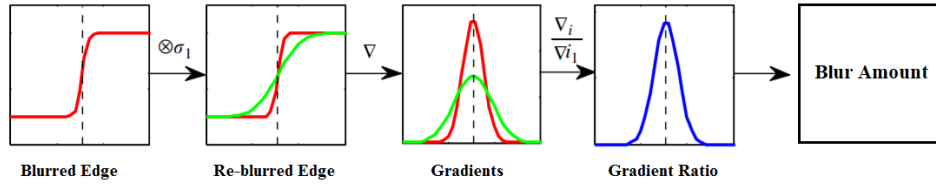$$B(z) = Sharp(z) \otimes Psf(z;\sigma) \tag{3}$$

FIGURE 1 Overview of the gradient ratio estimation proposed by Zhuo et al [?], the dashed line represents the edge location.

The standard deviation σ is proportional to COC(circle of confusion diameter C) which define the blurness in image. The point spread function can be assumed as a Gaussian amount in an image and we can model the defocus blur by convolving an edge pixel *z* with a Gaussian kernel *G(z; σ)*.

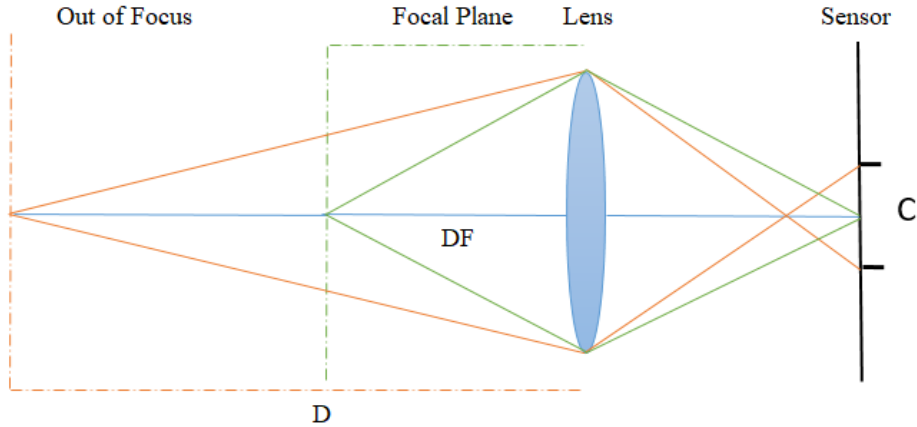$$B(z) = Sharp(z) \otimes G(z;\sigma) \tag{4}$$

FIGURE 2 Thin lens model.

3 | PROPOSED METHOD

We offered a novel system for modeling the defocus blur estimation. The defocus blur in an image is caused by the convolution of a sharp image and PSF (point spread function), approached by using the traditional Gaussian function. For defocus blur estimation most of the previous researches and even states of the art methodologies uses the Gaussian function for re-blurring the reference image. Using Gaussian is sensitive towards sparse map and full defocused map in ratio based methods and further causes some loss of information at weak edge locations. We are interested to estimate the blur around edges, and cannot afford the loss of some important information which is local to edges. For addressing this issue fast repeated averaging filters function is introduced and further incorporated it with the superpixels segmentation for attaining the full defocus blur map. Repeated averaging filters function approximates a good estimate of the Gaussian using some amount of sigma which is computationally

low cost and more than the traditional Gaussian function. Kovesi [33] suggested a method which presented an alternative to the traditional Gaussian function by applying the repeated averaging filters through integral image at very low computational cost. The procedure in [33] advocates that repeated filtering with averaging filters can be used for fast Gaussian filtering approximations. We adopted the advocated approach. First applied averaging filters repeatedly to the input image. In the process, the input image converted into an integral image. Mathematically integral image is defined as follows

$$\sum_{abcd} = S(x_c, y_c) - S(x_b, y_b) - S(x_d, y_d) + S(x_a, y_a) \tag{5}$$

An ideal averaging filter width is defined by assuming Equation (8). For defocus blurs estimation the edges are boundaries which are of interest for blur recovery. Applying the normal Gaussian for the blur process can harm some edge information in the re-blur process. The supremacy of this filter is that it is a movable filter, unlike the Gaussian kernel which is symmetrical. We recovered a sparse map with better edges from gradient ratios using the repeated averaging filters prior. Propagating the sparse map is a time consuming task. For fast sparse map propagation, we implemented the method of Chen [27]. Where a simple linear iterative clustering (SLIC) superpixel procedure [34] is castoff for over-segmenting the image. For identical objects of interest in images region based segmentation preferred and worked well relying on intensity thresholding. But for images having noise, texture and clutter can limit the performance of region based segmentation. For instance, the segmentation approaches which purely rely on intensity thresholding results in too fine or too rough segmentation for segmenting the non-identical objects of interests, which is categorized as under-segmentation and over-segmentation [35]. Over-segmentation is much faster than the traditional approaches used formerly for propagating the sparse map with an additional feature of transductive inference. Therefore the over-segmentation practice is introduced where the segmented objects from the background are being segmented from already segmented objects, which is useful for selecting the boundaries of the importance of objects in images. Our proposed algorithm is shown in Figure 3.

3.1 | Adopting the fast Gaussian approximation model

To achieve efficient Gaussian approximation via multiple averaging, specific averaging filters needed for the approximation of Gaussian. The standard deviation of an averaging filter of width w is given as

$$\sigma_{av} = \sqrt{\frac{W^2 - 1}{12}} \tag{6}$$

Performing n averaging's with the same filter the variances produce overall filtering effects equivalent to the standard deviation of

$$\sigma_{av} = \sqrt{\frac{(n)W^2 - n}{12}} \tag{7}$$

From this, one can compute the ideal width of the averaging filter that is equivalent to the normal Gaussian distribution given as

$$W_{ideal} = \sqrt{\frac{12\sigma_{av}^2}{12} + 1} \tag{8}$$

For further manipulations and parameters settings one can refer to [33]. So it is assumed that this ideal averaging filter is equivalent to the traditional Gaussian kernel. The mathematical representation of this assumption given as

$$W_{ideal} = \sqrt{\frac{12\sigma_{av}^2}{12} + 1} \approx G(z; \sigma_{av}) \tag{9}$$

3.2 | Modelling defocus blur estimation with repeated averaging filters

Gradient based defocus estimation has two phases; one to estimate defocus blur at edge locations; in the second phase, the computed sparse defocus blur propagation to the entire image. Our proposed method has outcomes in both phases. The first effect
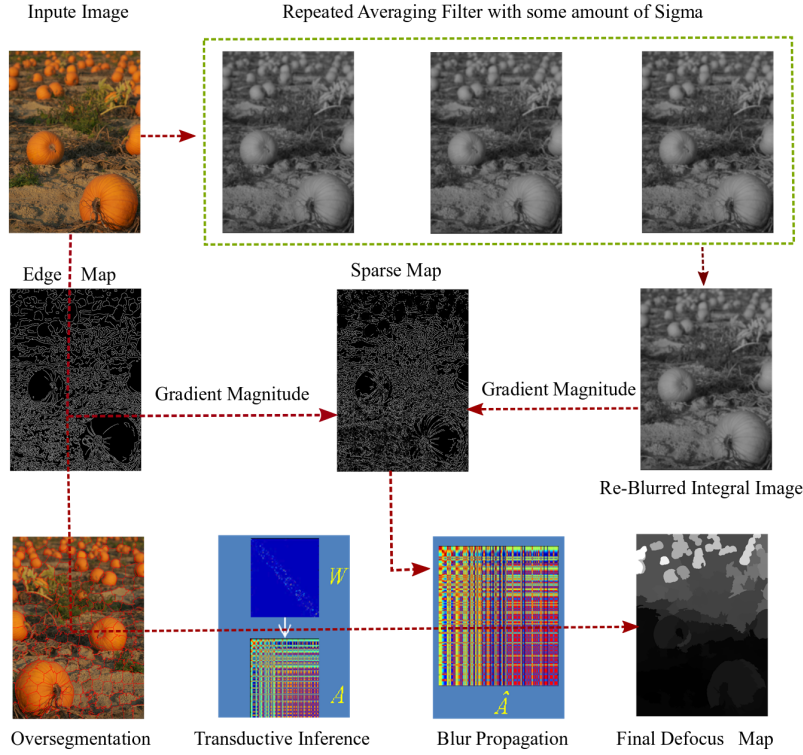
FIGURE 3 Our proposed algorithm. Relating the averaging filters repetitively via integral images, which outcomes in a reblurred integral averaged image. Taking the ratio of gradient magnitudes of input and reblurred image yields the sparse map with respect to the edge map. The robust Over-segmentation process is applied to obtain the weighted matrix. A transductive inference is used to calculate the affinity matrix. Considering the superpixels and affinity information the sparse is propagated into the whole image and finally, estimated the final defocus map.

is, by repeated averaging filter method decreases the computation time of sparse defocus map and second is, it also produces the better visualization of the final defocus map on the basis of obtained sparse map. We have an input defocus image; our first task is to detect edges. We applied the state of the art canny edge detector [36]. In the next step, we re-blurred the reference image by proposed repeated averaging filters with some amount of sigma and replaced it as an alternative to the traditional Gaussian function. Re-blurring the edge pixels using our repeated averaging filtering method, the gradient of the re-blurred edge is represented as

$$\nabla B(z) = \nabla(E(z) \otimes G(z; \sigma_{av})) \tag{10}$$

From Equation (1)

$$\nabla B(z) = \nabla(AlphaU(z) + Beta) \otimes G(z; \sigma) \otimes G(z; \sigma_{av}) \tag{11}$$

$$= \frac{\alpha}{\sqrt{2\pi(\sigma^2 + \sigma_{av}^2)}} exp \frac{-z^2}{\sqrt{2(\sigma^2 + \sigma_{av}^2)}} \tag{12}$$

Equation (9) proposes that repeated averaging filter is approximately equivalent to the traditional Gaussian function so Equation (11) can be modified by considering Equation (1) and Equation (9). In Equation (12), σ_{av} signifies the standard deviation of the repeated averaging filter re-blur kernel. From the technique of Zhuo [19], gradient magnitude ratio of the actual blurred edge and the reblurred edge is maximum by value at edge locations which can be modified as

$$R = \frac{|\nabla b(z)|}{|\nabla b(z) \otimes G(z; \sigma_{av})|} = \sqrt{\frac{\sigma^2 + \sigma_{av}^2}{\sigma^2}} \tag{13}$$

This suggest that we can estimate the unknown blur σ from the gradient magnitude ratio at the edge locations which can be represented as

$$\sigma = \frac{\sigma_{av}^2}{\sqrt{R^2 - 1}} \tag{14}$$

Where av is known quantity and R can be derived from gradient magnitudes.

3.3 | Sparse map propagation

For propagating the sparse map, the super pixels creation SLIC algorithm [36] and transductive inference [37] are followed. First a weighted matrix W is constructed by over-segmenting an image and super pixel set is defined as

$$S = \{s_1, s_2, ..., s_N\} \tag{15}$$

Keeping the super pixel S set in view a weighted connected graph is defined as $G = (S, \varepsilon, \omega)$. S is the vertex super pixel set and ε is the edge set which contains adjacent superpixels where every vertex S_i represents a single superpixel in S and edge ε_{ij} belongs to ε representing the adjacency relationship between S_i and S_j. A weight function is defined as $\omega : \varepsilon \to [0, 1]$ which further corresponds to ω_{ij} with respect to each edge ε_{ij} for similarities and a final weight matrix is obtained as $W = [\omega_{pq}]_{N \times N}$ The acquired matrix W which is similarity between two adjacent superpixels. By transductive inference a N-by-N an affinity matrix is further defined as

$$A = (D - \gamma W)^{-1} I \tag{16}$$

Where I is N-by-N identity matrix. D directs to a diagonal matrix, W is diagonal entry, γ is a parameter in the range $(0, 1)$. The affinity matrix encrypts the transductive resemblance between superpixels and consequently high chances of adjusting the defocus blur for superpixels pairs. An initial defocus blur f_s for every superpixel can be defined as

$$f_{si} = median_{x \epsilon E_i}\{f_x\} \tag{17}$$

Where E_i is set of interior edge pixels. Median is used to avoid the outliers. f_x is computed by Equation (14) and finally considering the defined affinity information the defocus blur propagation is defined as:

$$\widehat{f_{si}} = \widehat{A}.[f_{s1}, f_{s2}, ..., f_{sn}]^T \tag{18}$$

$\widehat{A}$ is modified affinity matrix. The Equation (18) defines defocus blur and shows that the defocus blur derived from all superpixels except from those superpixels which have no edge pixels. As a result the sparse map is propagated into the whole image.

4 | RESULTS AND DISCUSSIONS

The defocus blur map estimation mainly focused on the sparse map generation and propagation of sparse map, to get full defocus blur map. It is observed that blur in a defocus image usually occurs and estimated around the edge pixels. Adopting the proposed modified Gaussian function, it is experimentally proved that a better sparse map is estimated so therefore gives good visual estimates of the full defocus blur of the blurred image.

For our experimentation the system specification is ASUS machine with Intel Core i7-6700HQ 2.60 GHz CPU running with Installed memory (RAM) 8.00 GB, with MATLAB 2016b under windows 10. We used the dataset for blurry images which are collected from previous related literature [4,19]. Our scheme first transforms the input image into an integral image and further we apply the repeated averaging filters method referred as box-like filtering. Box Filtering and summed area tables also known as integral images. Summed area tables is the process of cumulating and summing the pixels values along the rows and columns of the image. Therefore the sum of the rectangular region is computed using O(1) independent of its size. The summed area tables or integral images useful to convolve an image very fast [38] and calculations can be decreased. Bay et al [39] exploited that these filters are also convenient for constructing filters like Haar and one can approximate first and second order derivative Gaussian filters.

Our recommended approach performs two operations first is to make use of integral image and then apply some blur, alternative to the traditional Gaussian filtering. Acquiring the repeated averaged reblurred integral image we evaluated the gradient magnitudes of the input and re-blurred images. Taking the gradient magnitudes of both the input and blurred image, we calculated the gradients ratio which resulted in sparse defocus map. As the previous methods used the traditional Gaussian filter for re-blurring the input image which causes loss of weak edges. Contrary, our adopted repeated averaging filter preserve more of the weak edges information and eventually we get fast and visually good sparse map which is important for recovering the full defocus map.

For sparse map propagation, we utilized the over-segmentation method to create the super-pixels by SLIC algorithm [34] and transductive inference [37] as in the method of Chen [27], which surpasses many states of the art methods proposed previously. We observed that repeated averaging filters produced better visual estimates of the blur even for high precision images and the computational time is less than 0.90 seconds for 800x800 image. We set sigma as 1.8 and 2 and applied 3 to 4 repeated averaging filters for performing our experiments. Applying at least three filters achieves the same approximation for the traditional Gaussian distribution. Using four repeated averaging filters the approximation to Gaussian becomes very decent [33]. To evaluate our experimentation we kept sigma amount as 1.8 or above because our proposed method considers the sigma amount higher or equal to 1.8. Results of the sparse map as shown in Figure 4.

FIGURE 4 Shows the sparse map comparison, where top row is input image, the second row is Zhuo [19] method, and the third row is the sparse map of our proposed method with much of edge information preserved as compared to others.

Previously most of the methods focused only on the second phase of propagating the sparse map. But in our method we targeted the first phase of sparse map generation which can further causes better visual estimates of the defocus blur. The repeated averaging produced fast and better sparse map compared to the previous techniques. Our experimental assessment provides qualitative analysis, computational analysis, and quantitative analysis which is compared further with the methods of Chen [27], Zhuo [19], Jiang [4], Shi [7] and Shi [2].

4.1 | Qualitative Analysis

To visualize the outputs better the defocus blur of all methods are normalized to the range of [0, 1] as in Chen [27] scheme which advises that higher intensity values are pointing towards stronger defocus blur. The qualitative results can be shown in Figure 5. (a) is input image, (b) are our evaluated results on the basis of 4 repeated averaging filters with sigma amount of 1.8. (c), (d), (e), (f), (g) are the qualitative analysis of Chen [27], Zhuo [19] [19], Jiang [4], Shi [7] and Shi [2], respectively.
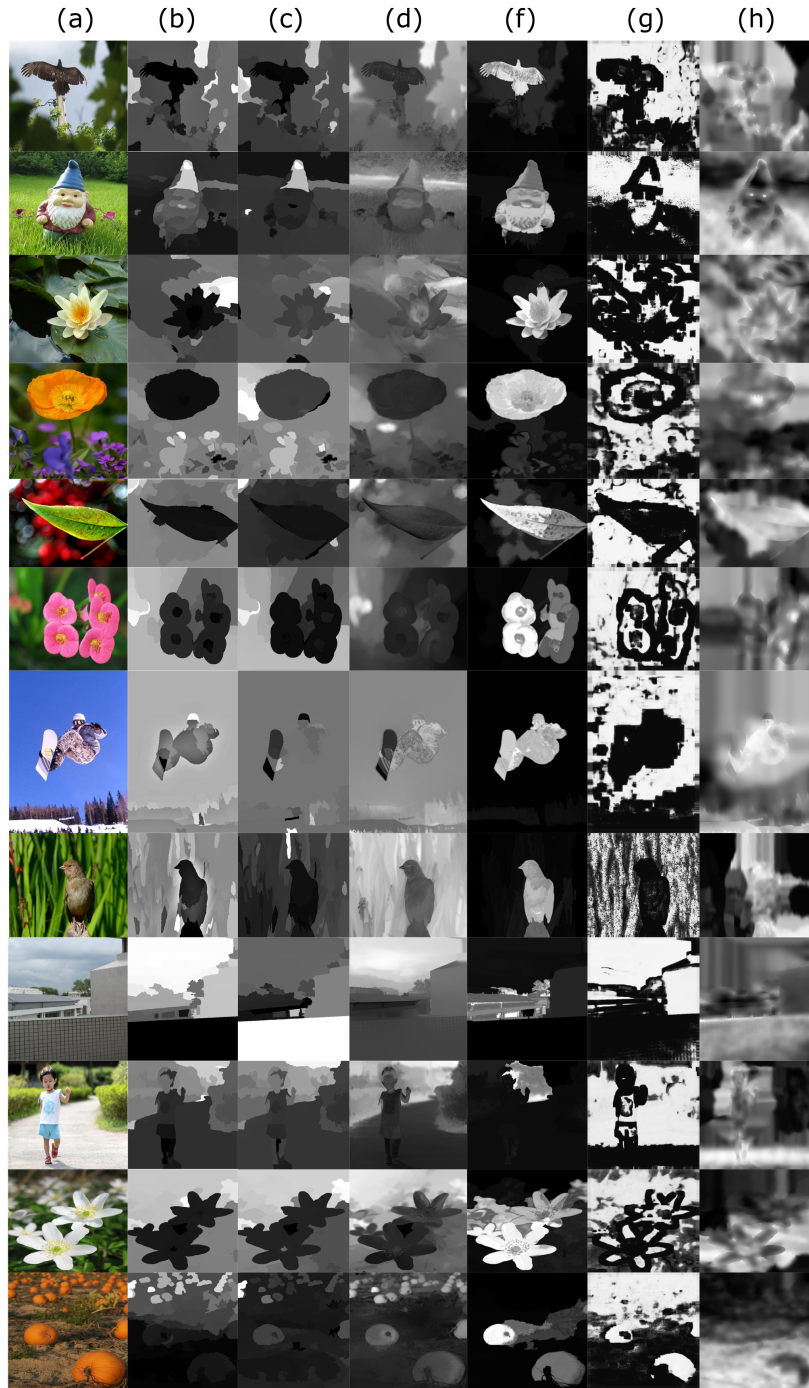
FIGURE 5 Qualitative Evaluation.

4.2 | Quantitative Analysis

Pratt's Figure of Merit (PFOM) measure [40] is used to provide further quantitative analysis for the edges in the sparse map. Pratt's introduced a method, figure of merit by analyzing and balancing errors in the process of edge detection, which is given as

$$R = \frac{1}{I_N} \sum_{i=1}^{I_A} \frac{1}{1 + ad^2} \tag{19}$$

TABLE 1 Summary of SSIM and MSE measures

	Proposed		Chen et al [27]		Zhuo et al [19]		Shi-1 et al [7]		Shi-2 et al [2]		Jiang et al [4]	
Image	SSIM	MSE	SSIM	MSE	SSIM	MSE	SSIM	MSE	SSIM	MSE	SSIM	MSE
1	0.5336	6025	0.5134	8991	0.4712	8247	0.3204	11247	0.5274	4892	0.1909	14243
2	0.3384	4770	0.3038	8099	0.0886	5035	0.0923	15909	0.2463	5964	0.1468	10341
3	0.6513	3516	0.4613	5444	0.2617	6492	0.2239	13098	0.3436	7197	0.3419	5773
4	0.5099	4378	0.4816	9148	0.4770	4334	0.2160	10242	0.4619	5946	0.2868	3112
5	0.4711	4804	0.4455	4672	0.3065	5471	0.1671	20934	0.2816	8159	0.4562	3110
6	0.6105	4929	0.3953	13745	0.5464	5331	0.2310	15667	0.5226	4702	0.2667	3809
7	0.6931	3111	0.7122	3350	0.5892	3953	0.2645	15547	0.5981	3814	0.0553	15070
8	0.3103	4588	0.4443	3480	0.3721	12740	0.1203	6768	0.2995	7865	0.1483	6648
9	0.4891	6975	0.3338	18902	0.2905	21576	0.3938	16018	0.3491	11817	0.1164	28720
10	0.5594	1933	0.4373	15404	0.5663	2201	0.3586	7458	0.4665	6552	0.1157	15922
11	0.6068	9841	0.3867	16053	0.2971	15204	0.3199	12436	0.3404	11848	0.4604	4336
12	0.5009	5513	0.3264	3951	0.5328	1948	0.2131	11159	0.3138	6264	0.1364	6438
Average	0.5228	5031	0.4368	9269	0.3999	7711	0.2434	13040	0.3959	7085	0.2268	9793

Where $I_N = max I_I, I_A$. I_I is the ideal edge map and I_A is an actual edge map, a is scaling constant, d represents separation distance for actual edge points which is normal to a line of ideal edge points. For this tenacity first, we applied the Sobel operator [40] on edges and assumed it our reference or ideal edge map. Similarly, the sparse map edges are supplied as detected edges or actual edges to the Pratt's Figure of Merit (PFOM). Using the PFOM measure our method have much edge preserving efficiency compared with the traditional Gaussian filter which is illustrated in the Figure 7.
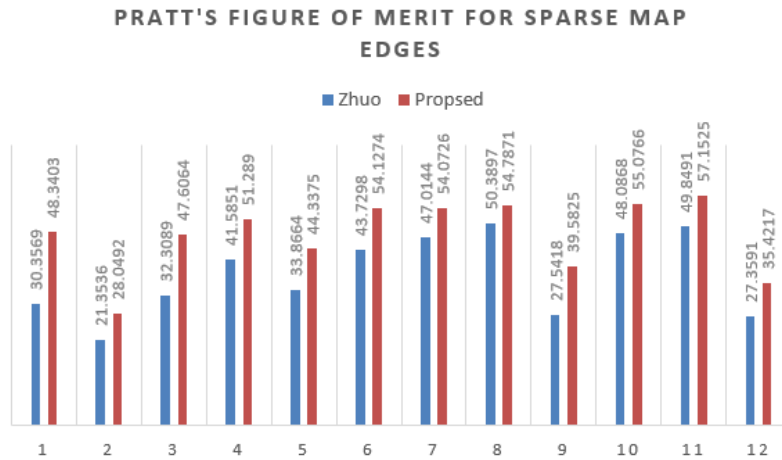

FIGURE 6 The Pratt's Figure of Merit (PFOM) measure for 12 images. The figure compares the sparse map edges obtained from our method and Zhuo [19] proposed method. They used the traditional Gaussian and affects the edges in the sparse map while our method preserves much of edge information and hence proved by the Pratt's Figure of Measure (PFOM).

Further, we evaluated the structural similarity (SSIM) index and mean squared error (MSE) measures, our method surpasses all the comparative methods. The SSIM and MSE measures are summarized in Table 1. For SSIM and MSE evaluation, the input RGB image is converted into a grayscale image and then passed the grayscale image as a reference image to SSIM and MSE function. Likewise a Perception based Image Quality Evaluator (PIQE) no-reference image quality score is also derived which documented in Table 2.

TABLE 2 Perception Based Image Quality Evaluator (PIQE) evaluatiion

Perception Based Image Quality Evaluator (PIQE)- no refrence image quality score					
Image	**Proposed**	**Chen et al [27]**	**Zhuo et al[19]**	**Shi-1 et al[7]**	**Shi-2 et al[2]**	**Jiang et al[4]**
1	87.7005	86.4132	46.2867	80.5136	79.9791	69.4261
2	90.7279	88.4004	27.8127	77.1165	89.3618	70.9878
3	93.8429	88.0999	45.0769	81.0404	91.2433	74.1297
4	87.4708	86.9204	54.9082	69.2991	81.4296	68.2903
5	88.0421	87.6264	37.5623	75.9532	90.2347	56.7498
6	91.7564	88.8902	47.4429	79.2945	93.7210	83.8199
7	94.2218	87.2215	43.0590	78.3703	84.6277	56.5710
8	70.7032	87.7970	29.5122	45.5111	54.5174	59.3121
9	88.5801	86.8828	29.9651	67.9904	89.2088	82.0605
10	94.5987	87.3023	51.7024	71.7990	91.1849	78.2735
11	93.9099	88.7243	48.3920	71.1264	92.5007	74.6482
12	90.7376	87.2059	37.8502	53.6065	90.8149	69.3145
Average	89.35	87.62	41.63	70.96	85.73	70.29

4.3 | Computational Analysis
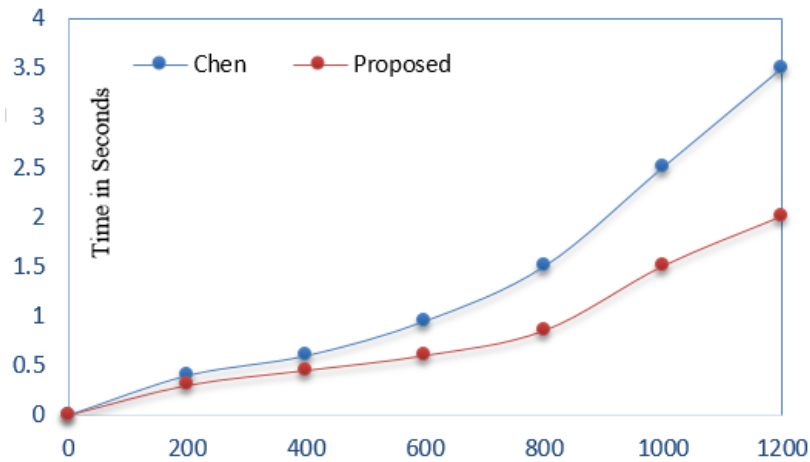
FIGURE 7 Proposed method computational comparision with Chen et al [27].

5 | CONCLUSION AND FUTURE PERSPECTIVES

Our technique is based on repeated averaging filters via integral images to replicate traditional Gaussian function which is used excessively in most of the preceding methods of defocus blur map recovery. The modified Gaussian function blurs the input image very fast which generates a better sparse map at low computational cost as compared to the traditional Gaussian function with much edge perseverance which affects the final estimates of the defocus map visually. The reason behind this is that it converts the input image to integral image and the post processing can be done fast as compared to the previous traditional methods. The repeated averaging filter provides faster aid to the state of the art techniques and made its computational time less than 0.90 seconds for even high precision defocus blurry images. For our future work we will use the guided filter for sparse map refinement and for faster propagation of the sparse map we will consider the over-segmentation method of 'FLIC' for superpixel
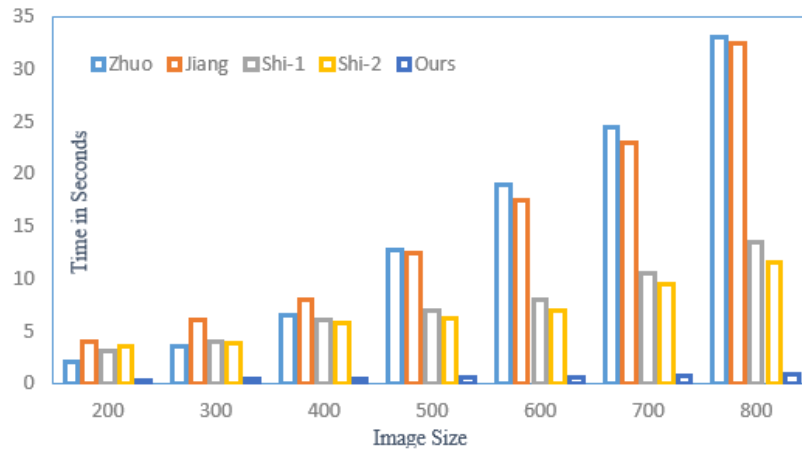
FIGURE 8 Comparison with Zhuo [19], Jiang [4], Shi-1 [7] and Shi-2 [2].

segmentation or alternatively the object level regions (ex, Mask-RCNN) instead of superpixels. Further the repeated averaging filter can be used for underwater images de-hazing or outdoor image de-hazing.

5.1 | Acknowledgements

References

1. Tang C, Hou C, Song Z. Defocus map estimation from a single image via spectrum contrast. *Optics letters.* 2013;38(10):1706-1708.

2. Shi J, Xu L, Jia J. Just noticeable defocus blur detection and estimation. *Proceedings of the IEEE Conference on Computer Vision and Pattern Recognition.* 2015.

3. Aslantas V. A depth estimation algorithm with a single image. *Optics express.* 2007;15(8):5024-5029.

4. Jiang P, Ling H, Yu J, Peng J. Salient region detection by ufo: Uniqueness, focusness and objectness. *Proceedings of the IEEE international conference on computer vision.* 2013.

5. Rhemann C, Rother C, Kohli P. A spatially varying PSF-based prior for alpha matting. *Computer Vision and Pattern Recognition (CVPR), IEEE Conference.* 2010.

6. Shi J, Tao X, Xu L, Jia J. Break ames room illusion: depth from general single images. *ACM Transactions on Graphics (TOG).* 2015;34(6):255.

7. Shi J, Xu L, Jia J. Discriminative blur detection features. *Proceedings of the IEEE Conference on Computer Vision and Pattern Recognition.* 2014.

8. R. Fergus R, Singh B, Hertzmann A, Roweis S. Removing camera shake from a single photograph. ACM transactions on graphics (TOG). *Computer Vision and Pattern Recognition (CVPR), 2010 IEEE Conference on. IEEE.* 2010: 1110–1117.

9. Zhang Y, Keigo H. Blur processing using double discrete wavelet transform. *Proceedings of the IEEE Conference on Computer Vision and Pattern Recognition.* 2013.

10. Elder J, Zucker S. Local scale control for edge detection and blur estimation. *IEEE Transactions on pattern analysis and machine intelligence.* 1998;20(7):699-716.

11. Bae S, Durand F. Defocus magnification. *Computer Graphics Forum. Oxford, UK: Blackwell Publishing Ltd.* 2007;26(3):571-579.

12. Namboodiri V, Chaudhuri S. Recovery of relative depth from a single observation using an uncalibrated (real-aperture) camera. *Computer Vision and Pattern Recognition (CVPR). IEEE Conference.* 2008.

13. Peng Y, Zhao X, Cosman P. Single underwater image enhancement using depth estimation based on blurriness. *Image Processing (ICIP), 2015 IEEE International Conference.* 2015.

14. P. Favaro P, Soatto S, Burger M. Shape from defocus via diffusion. *IEEE transactions on pattern analysis and machine intelligence.* 2008;30(3):518-531.

15. Zhou C, Cossairt O, Nayar S. Depth from diffusion. *Computer Vision and Pattern Recognition (CVPR), 2010 IEEE Conference on. IEEE.* 2010: 1110–1117.

16. Pentland A. A new sense for depth of field. *IEEE transactions on pattern analysis and machine intelligence.* 1987;4:523-531.

17. Favaro P, Soatto S. A geometric approach to shape from defocus. *IEEE Transactions on Pattern Analysis and Machine Intelligence.* 2005;27(3):406-417.

18. Liu R, Li Z, Jia J. Image partial blur detection and classification. *Computer Vision and Pattern Recognition,CVPR,IEEE Conference.* 2008.

19. Zhuo S, Sim T. Defocus map estimation from a single image. *Pattern Recognition* 2011;44(9):1852-1858.

20. Tai Y, Brown M. Single image defocus map estimation using local contrast prior. *Image Processing (ICIP),16th IEEE International Conference IEEE.* 2009.

21. Zhu X, Cohen S, Schiller S. Estimating spatially varying defocus blur from a single image. *IEEE Transactions on image processing.* 2013;22(12):4879-4891.

22. Wang J, Gray R. Unsupervised multiresolution segmentation for images with low depth of field. *IEEE Transactions on Pattern Analysis and Machine Intelligence.* 2001;23(1):85-90.

23. Kim C. Segmenting a low-depth-of-field image using morphological filters and region merging. *IEEE Transactions on Image Processing.* 2005;14(10):1503-1511.

24. Kovacs L, Sziranyi T. Focus area extraction by blind deconvolution for defining regions of interest. *IEEE transactions on pattern analysis and machine intelligence.* 2007;29(6):1080-1085.

25. Saxena A, Chung S, Ng A. Learning depth from single monocular images. *dvances in neural information processing systems.* 2006.

26. Pi F, Zhang Y, Lu G, Pang B. Defocus blur estimation from multi-scale gradients. *Fifth International Conference on Machine Vision (ICMV 2012): Computer Vision, Image Analysis and Processing. Vol. 8783. International Society for Optics and Photonics, 2013.* 2013;22(9):3703-3714.

27. Chen D, Chen H, Chang L. Fast defocus map estimation. *Image Processing (ICIP),International Conference on. IEEE.* 2016.

28. Cao Y, Fang S, Wang Z. Digital multi-focusing from a single photograph taken with an uncalibrated conventional camera. *EEE Transactions on image processing.* 2013;22(9):3703-3714.

29. Zhang X, Wang R, Jiang X, Wang W, Gao W. Spatially variant defocus blur map estimation and deblurring from a single image. *Journal of Visual Communication and Image Representation .* 2016;35:257-264.

30. Karaali A, Jung C. Edge-Based Defocus Blur Estimation With Adaptive Scale Selection. *IEEE Transactions on Image Processing*. 2018;27(3): 1126-1137.

31. Andrès L, Salvador J, Kochale A. Non-parametric blur map regression for depth of field extension. *IEEE Transactions on Image Processing*. 2016;25(4): 1660-1673.

32. Hecht E. *Optics*. Addison Wesley. fourth ed. 2001.

33. Kovesi P. Fast almost-gaussian filtering. *Digital Image Computing: Techniques and Applications (DICTA), 2010 International Conference on. IEEE*. 2010.

34. Achanta R, Shaji A, Smith K, Lucchi A. SLIC superpixels compared to state-of-the-art superpixel methods. *EEE transactions on pattern analysis and machine intelligence*. 2012;34(11):2274-2282.

35. Peter E. understanding-oversegmentation-and-region-merging. *www.vision-systems.com/articles/print/volume-3/issue-12/departments/software-visions/understanding-oversegmentation-and-region-merging.html* 1998.

36. Canny J. A computational approach to edge detection. *IEEE Transactions on pattern analysis and machine intelligence*. 1986;6:679-698.

37. Zhou D, Bousquet O, Lal T, Weston J. Learning with local and global consistency. *Advances in neural information processing systems*. 2004.

38. Elboher E, Werman M. Efficient and accurate Gaussian image filtering using running sums[C]. *Intelligent Systems Design and Applications (ISDA),12th International Conference on IEEE*. 2012:897-902.

39. Bay H, Tuytelaars T, Gool L. Speeded up robust features. *European conference on computer vision. Springer, Berlin, Heidelberg*. 2006.

40. Sobel I, Gary F. A 3x3 isotropic gradient operator for image processing. *A talk at the Stanford Artificial Project in*. 1968:271-272.

41. Abdou I, Pratt W. Quantitative design and evaluation of enhancement/thresholding edge detectors. *Proceedings of the IEEE*. 1979;67(5):753-763.